Electronic Supplementary Material (ESI) for Journal of Materials Chemistry A.

Supporting Information

Controllable Crystal Orientation-Dependent Growth of High-Index Faceted Dendritic $NiC_{0.2}$ Nanosheets as High Performance Bifunctional Electrocatalysts for Over All Water Splitting

Haidong Yang, Sha Luo, Xinzhe Li, Shuwen Li, Jun Jin* and Jiantai Ma*

State Key Laboratory of Applied Organic Chemistry (SKLAOC), The Key Laboratory of Catalytic Engineering of Gansu Province, College of Chemistry and Chemical Engineering, Lanzhou University, Lanzhou, Gansu, 730000, P. R. China.

*E-mail: jinjun@lzu.edu.cn, majiantai@lzu.edu.cn

Tel.: +86-931-8912577

Fax: +86-931-8912582

Experimental section:

1、Estimation of electrochemically active surface areas (A_{echem})

Based on previous reports,[1, 2] cyclic voltammetry (CV) could be carried out in neutral media to probe the electrochemical double layer capacitance of various samples at non-Faradaic overpotentials as the means for estimating the A_{echem} of samples. Accordingly, a series of CV measurements were performed at various scan rates (4 mV s^{-1}, 8 mV s^{-1}, 12mV s^{-1}, 16 mV s^{-1}, etc.) in 0.1 to 0.2 V vs. RHE range, and the sweep segments of the measurements were set to 10 to ensure consistency. By plotting the difference in current density (J) between the anodic and cathodic sweeps (J_{anodic} - $J_{cathodic}$) at 0.15 V vs. RHE against the scan rate, a linear trend was observed. The slope of the fitting line is found to be equal-to-twice the geometric double layer capacitance (C_{dl}), which is proportional to the A_{echem} of the materials. Therefore, the A_{echem} of different samples can be compared with one another based on their C_{dl} values. However, it should be noted that this comparison makes sense only when the measurement of materials are carried out under same condition.

2、Measurements of electrochemical impedance spectroscopy (EIS)

EIS were performed under operating conditions (i.e., at a cathodic bias that drives rapid hydrogen evolution) according to the literature.[2] In our work, the initial electric potential was set as -0.25 V vs. RHE for direct comparison. A sinusoidal voltage with amplitude of 5 mV and scanning frequency values ranging from 100 kHz to 0.01 Hz were applied to carry out the measurements. The EIS response for each electrode were then fitted by a simplified Randles equivalent circuit, as showed in Figure 7 of main text, and the geometric values of series resistance (R_s) and charge transfer resistance (R_{ct}) are listed in Table S3.

3、Determination of Faradaic efficiency

The Faradic efficiency of a catalyst in HER or OER is defined as the ratio of the amount of H_2 or O_2, respectively, evolved during the experiments to the amount of H_2 or O_2 expected based on theoretical considerations.[2] For example, to measure the Faradic efficiency of HER, we carried out the following experiment. We collected the

evolved H_2 gas by water drainage method, and then calculated the moles of H_2 generated from the reaction with an ideal gas law. The purity of the generated gas was confirmed by gas chromatography (GC) analysis. As for the theoretical value, we assumed that 100% current efficiency occurs during the reaction, which means only the HER process takes place at the working electrode. We can then calculate the theoretical amount of H_2 evolved by applying the Faraday law, which states that the passage of 96485.4 C charge causes 1 equivalent of reaction.

4、Physical methods

Determination of the loading amount of dendritic $NiC_{0.2}$ nanosheets (d-$NiC_{0.2}$NS) grown on the Ni coated copper foil (Ni/CF) substrate, denoted m(d-$NiC_{0.2}$NS), was carried out as follows. (1) After synthesis of Ni/CF substrate, mass of Ni film grown on the CF equals the weight increment of CF (x mg), which can be directly obtained by comparing the weight of CF before and after the synthesis of Ni/CF. (2) After synthesis of d-$NiC_{0.2}$NS/Ni/CF sample, the weight increment (y mg) of Ni/CF substrate can be directly obtained by comparing the weight of Ni/CF substrate before and after the synthesis of d-$NiC_{0.2}$NS/Ni/CF. As a result, the m(d-$NiC_{0.2}$NS) of d-$NiC_{0.2}$NS/Ni/CF equals the y mg of weight increment divide geometric area of electrode ($A_{electrode}$), m(d-$NiC_{0.2}$NS) = y / $A_{electrode}$, with the value of 2.74 mg/cm^2.

To determine the mole ratio of Ni and C in the d-$NiC_{0.2}$NS of d-$NiC_{0.2}$NS/Ni/CF, the ICP-OES elemental analyses were performed on a Perkin Elmer (Optima-4300DV) ICP spectrometer. Using the ICP-OES elemental analyses, the total mole content of Ni (C(Ni-total)) in d-$NiC_{0.2}$NS/Ni/CF was measured, which enabled us to estimate the mole content of Ni and C in the d-$NiC_{0.2}$NS (C(Ni) and C(C)). As a result, C(Ni) = C(Ni-total) - x / 58.7, C(C) = [y - C(Ni) * 58.7] / 12.0, where 58.7 and 12.0 is the atomic

weight of Ni and C, respectively. Based on above results, the Ni and C loading amount of d-$NiC_{0.2}$NS on Ni/CF substrate was then calculated according to the equation: m(Ni) = C(Ni) * 58.7 / $A_{electrode}$ and m(C) = C(C) * 12.0 / $A_{electrode}$, respectively.

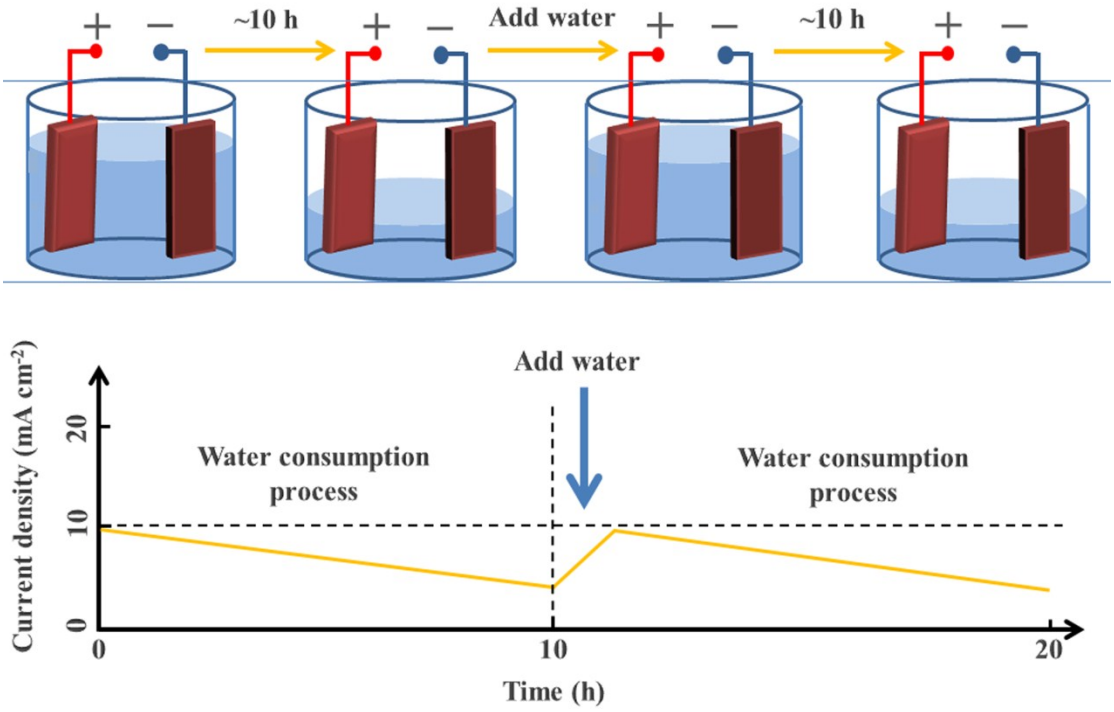

Scheme S1. Schematic explanation of the unstable I-t curves during electrocatalytic stability tests process for d-$NiC_{0.2}$NS/Ni/CF. During the water splitting process, water in the electrolyte was continuously consumed to generate hydrogen gas and oxygen gas, and then the liquid lever started to fall, which could result in a decrease of contact area between electrode and electrolyte, as well as the corresponding current intensity. After stability test for ~10 h, a certain amount of water was supplied into the electrolyte. Accordingly, the contact area between electrode and electrolyte was recovered to the original area, thus increasing the corresponding current intensity. Simultaneously, because the intrinsic area of the electrode is large, generating the relatively high yields of H_2 and O_2 (water consumption), which lead to an obvious fluctuation of the liquid level and the corresponding current density (Figure 4a).

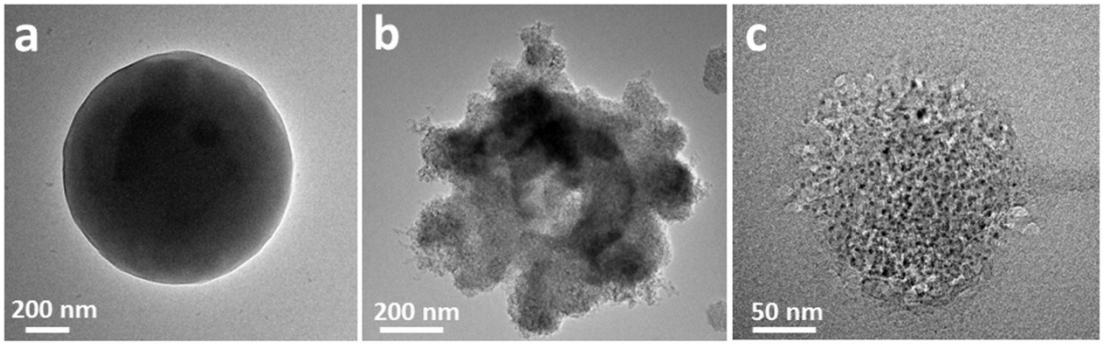

Figure S1. TEM images of PSP (a) before and (b), (c) after electrodeposition process. During the process, close contact between PSP and the cathode surface was allowed by assistance of ultrasounds. The ultrasonic bath and ohmic heating can generate local high-temperature and high-pressure environments. As a result of these extremely high energy conditions, PSP were violently burnt (i.e. carbonized).

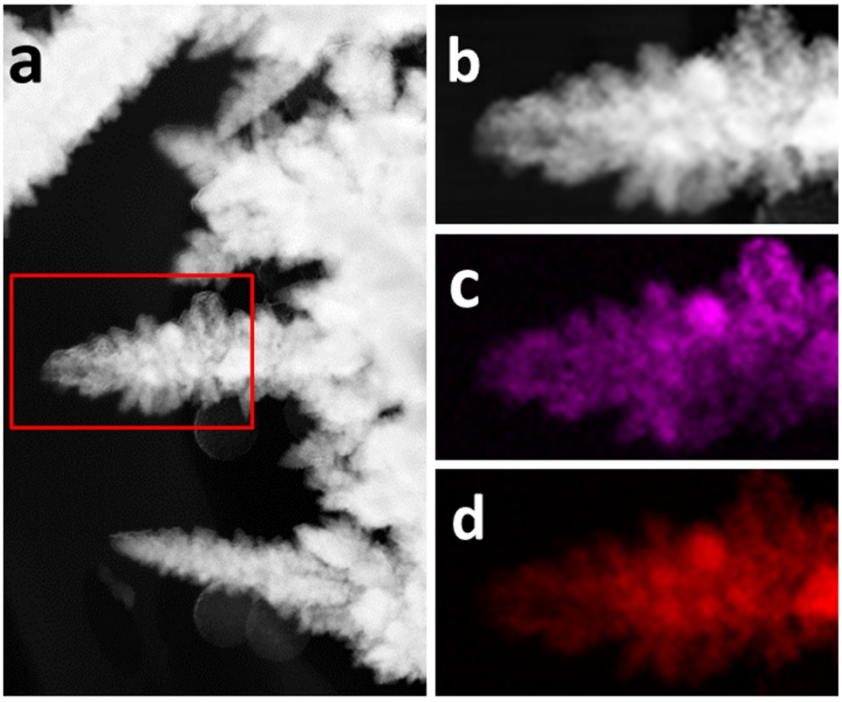

Figure S2. Elemental mappings of d-$NiC_{0.2}$NS, Ni (purple), C (red). Elemental analysis revealed that Ni and C were distributed uniformly throughout the entire dendritic nanosheet.

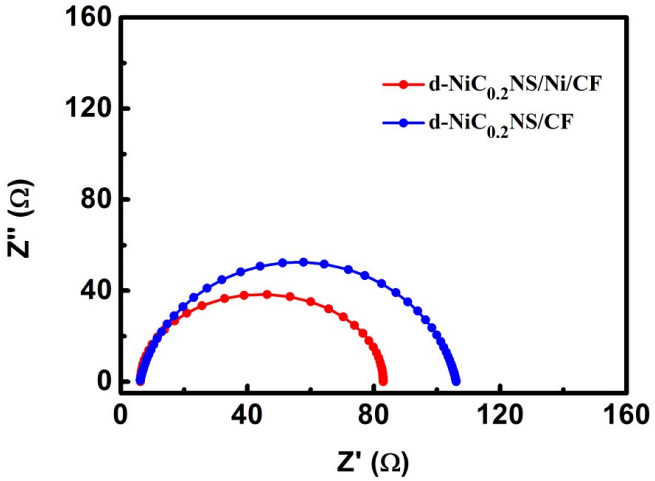

Figure S3. Nyquist diagrams of EIS for d-$NiC_{0.2}$NS/Ni/CF and d-$NiC_{0.2}$NS/CF.

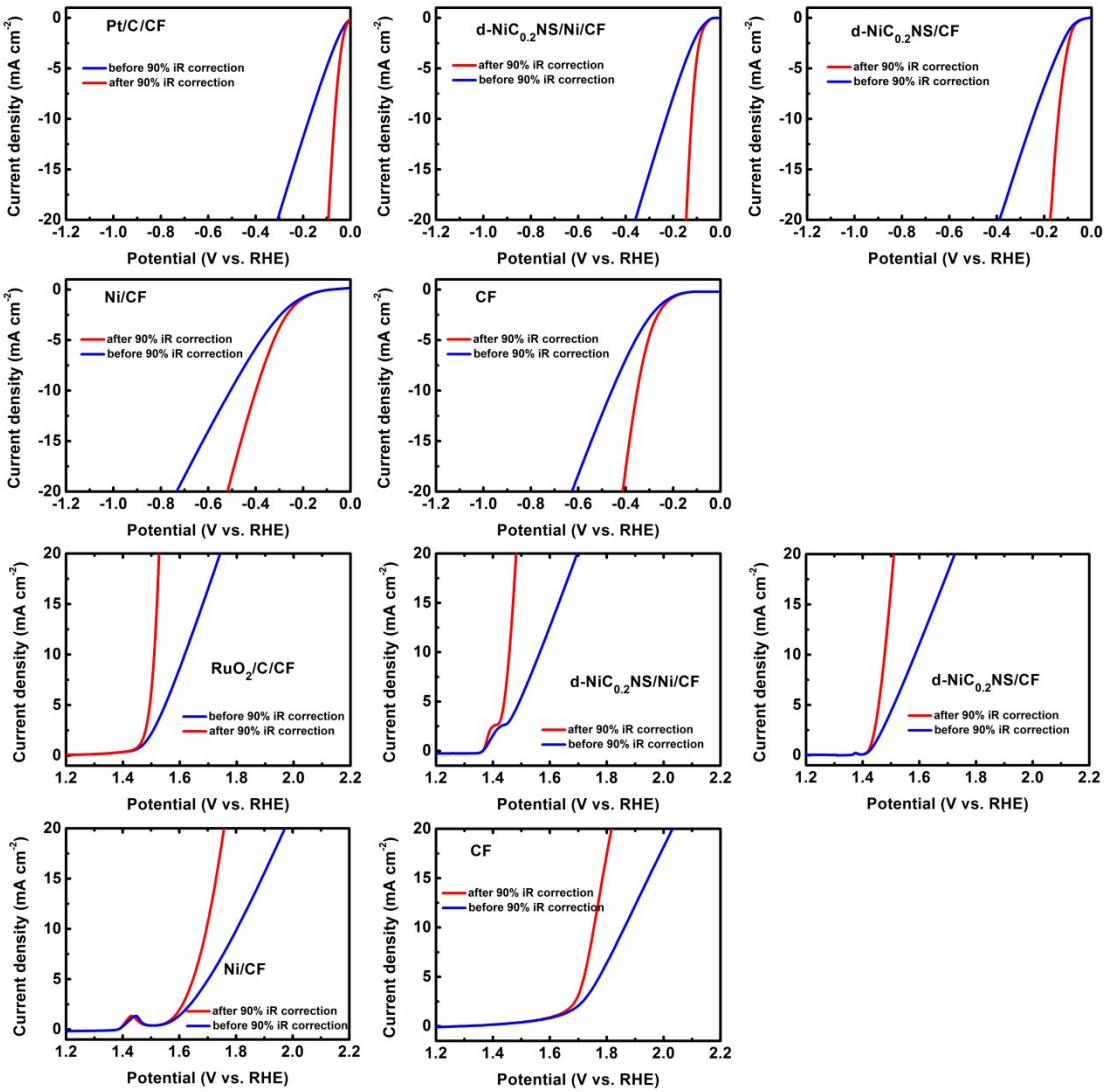

Figure S4. Respective HER and OER LSV curves of d-$NiC_{0.2}$NS/Ni/CF, d-$NiC_{0.2}$NS/CF, CF, Ni/CF, and Pt/C/CF or RuO_2/C/CF, before and after 90% iR compensation. 90% iR compensation[3,4] is an optimal compensation level to achieve best curve shape as well as avoid curve distortion by over-compensation,[5,6] and other corresponding electrochemical measurements were all based on this compensation percentage.

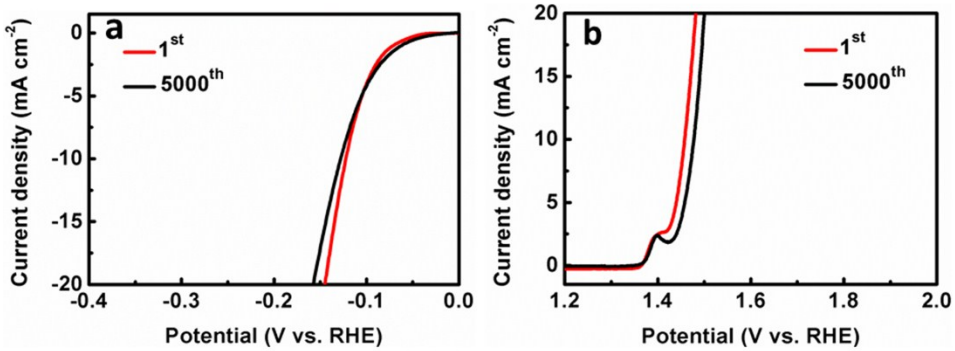

Figure S5. Polarization curves obtained over d-$NiC_{0.2}$NS/Ni/CF for (a) HER and (b) OER in 1 M KOH, before and after 5000 cycles.

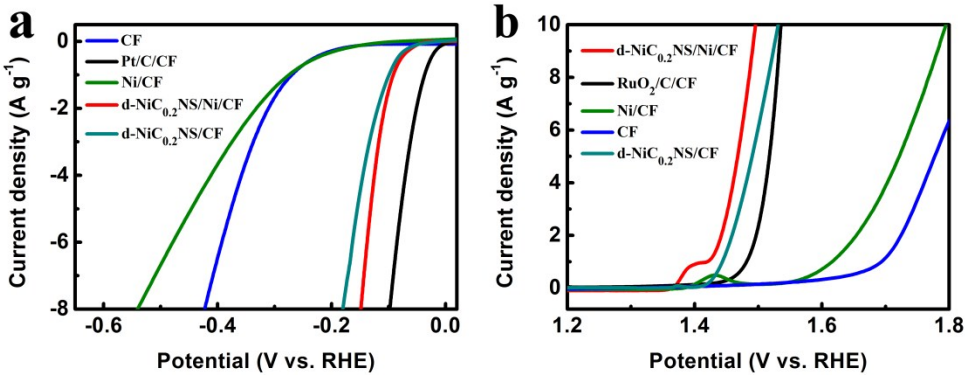

Figure S6. The (a) HER and (b) OER LSV curves of mass activity for d-$NiC_{0.2}$NS/Ni/CF, d-$NiC_{0.2}$NS/CF, CF, Ni/CF, and Pt/C/CF or RuO_2/C/CF. d-$NiC_{0.2}$NS/Ni/CF exhibits a remarkably electrocatalytic mass activity, which is slightly lower than that of Pt/C/CF for HER and higher than that of RuO_2/C/CF for OER, respectively. Based on the these results, we can conclude that d-$NiC_{0.2}$NS/Ni/CF is a versatile and efficient electrocatalyst for both HER and OER.

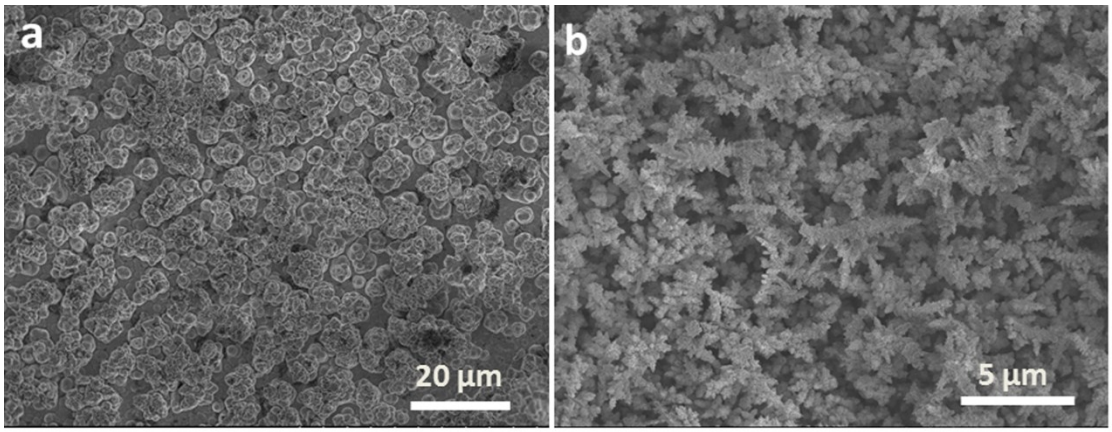

Figure S7. SEM images of as prepared (a) s-(-8)-100% and (b) s-(-10)-100%.

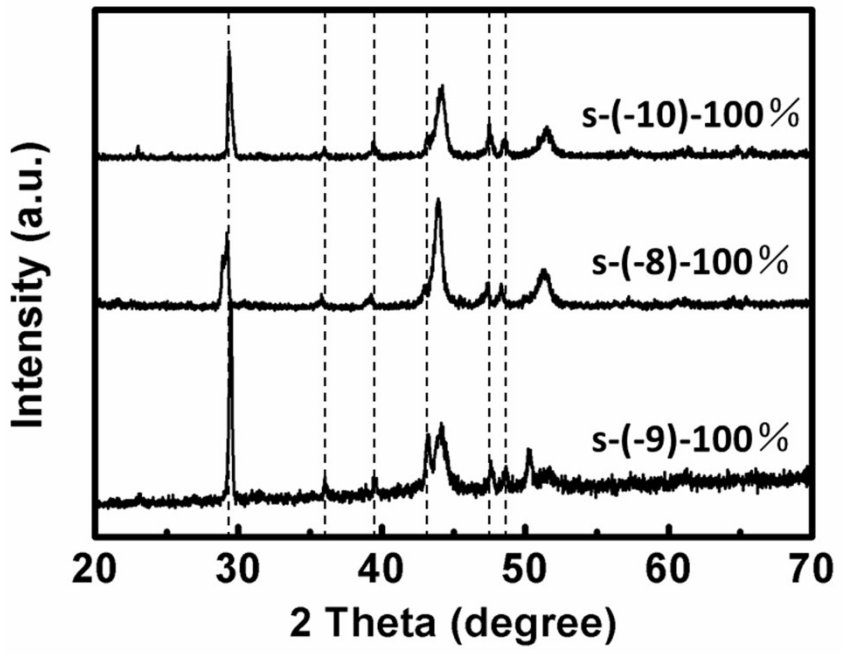

Figure S8. XRD spectras of as prepared s-(-10)-100%, s-(-9)-100% and s-(-8)-100%. The dashed lines represent the diffraction peaks of hexagonal NiC_x (JCPDS card no. 45-0979).

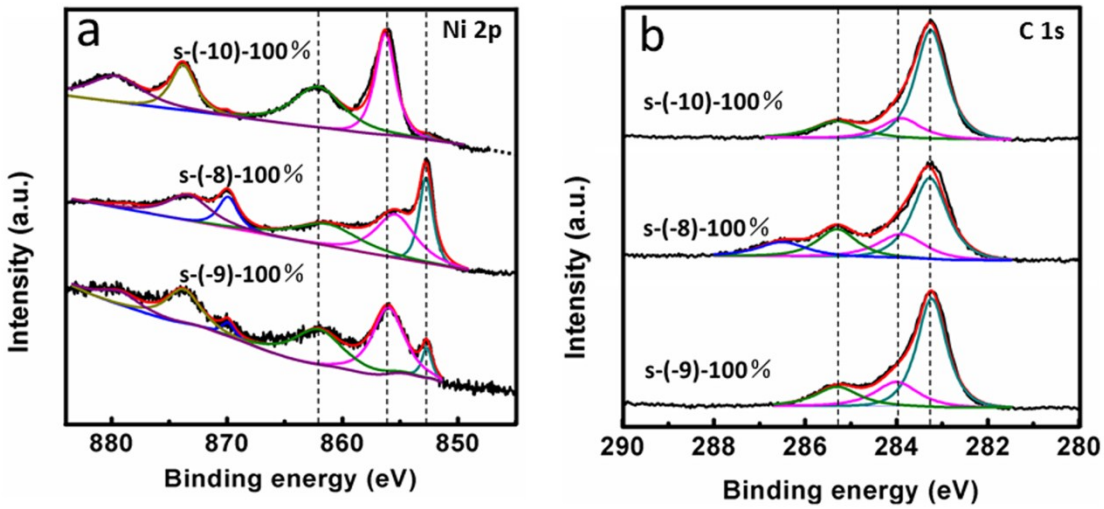

Figure S9. Ni 2p and C 1s XPS spectra for as prepared s-(-10)-100%, s-(-9)-100% and s-(-8)-100%. The dashed lines represent the peaks of metallic Ni, Ni^{2+}, Ni-C bonds, C–C (sp^3) bonds, and C–C (sp^2) or charge-transfer Ni–C* features in XPS patterns.[7,8]

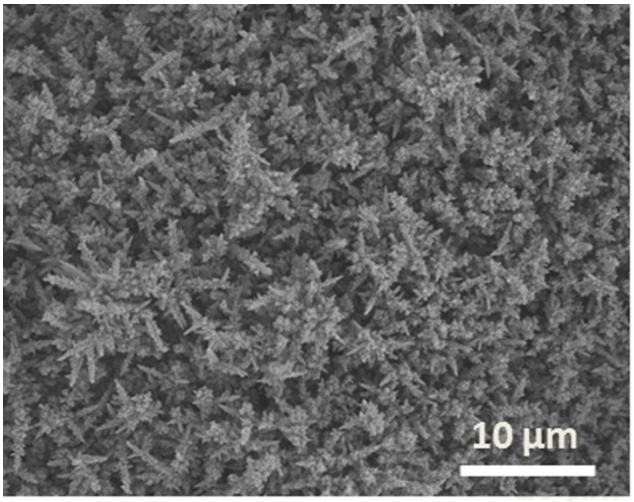

Figure S10. SEM images of as prepared s-(-9)-60%. The images show that the samples have a dendritic arrays morphology which is similar to s-(-9)-100%.

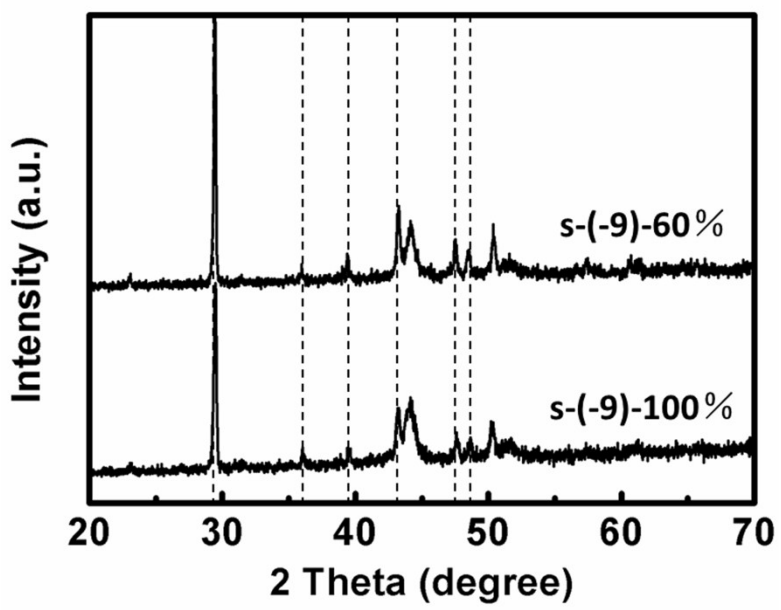

Figure S11. XRD spectras of as prepared s-(-9)-100% and s-(-9)-60%. The dashed lines represent the diffraction peaks of hexagonal NiC_x (JCPDS card no. 45-0979).

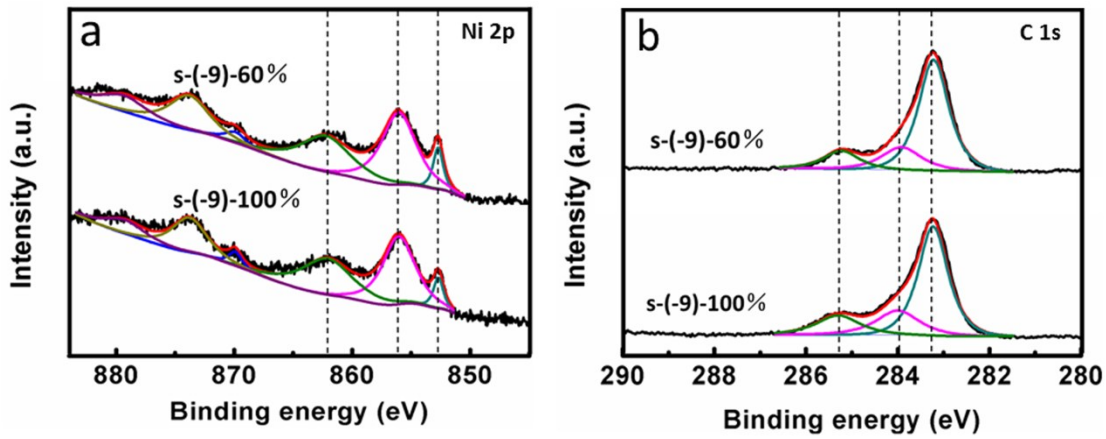

Figure S12. Ni 2p and C 1s XPS spectra for as prepared s-(-9)-100% and s-(-9)-60%. The dashed lines represent the peaks of metallic Ni, Ni^{2+}, Ni-C bonds, C–C (sp^3) bonds, and C–C (sp^2) or charge-transfer Ni–C* features in XPS patterns.

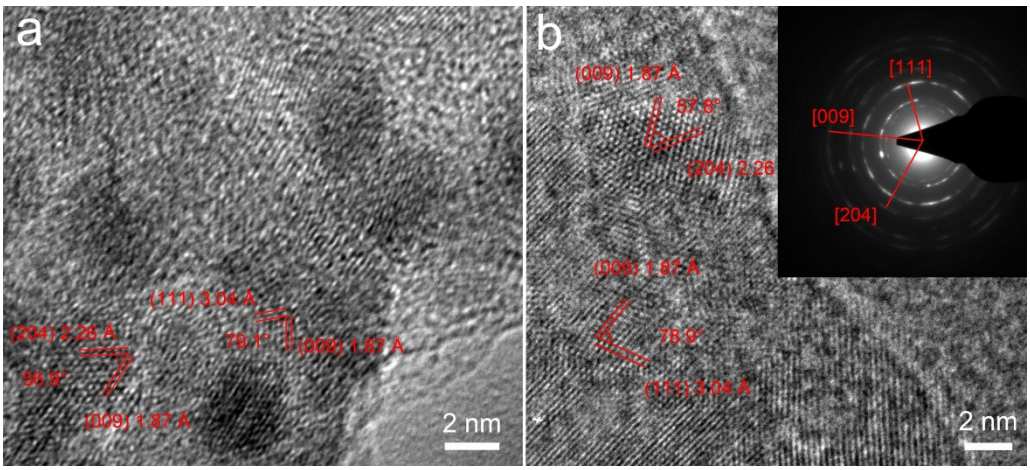

Figure S13. HRTEM images of as prepared s-(-9)-80%.

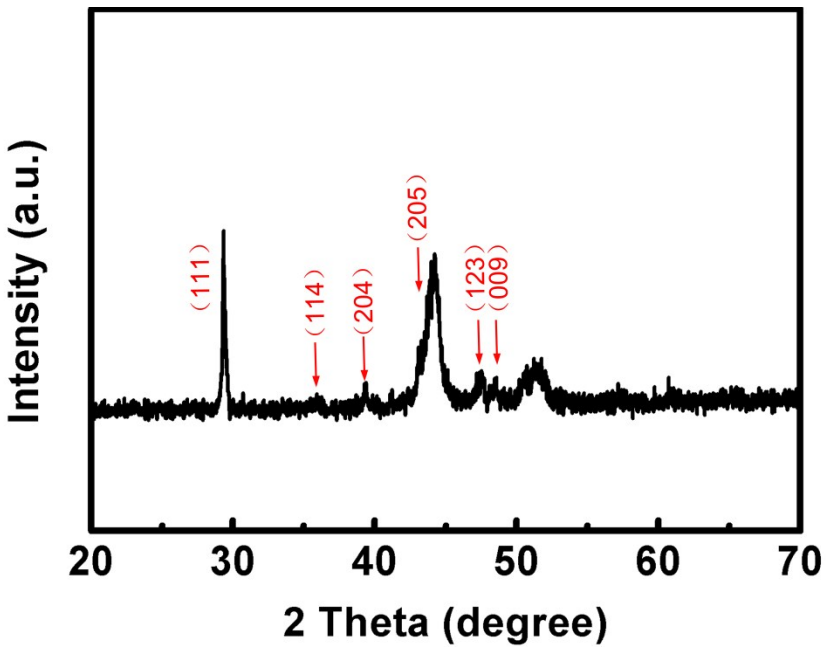

Figure S14. XRD pattern of as prepared s-(-9)-80%. The XRD pattern reveal that the s-(-9)-80% contains hexagonal NiCx, metallic Ni, and metallic Cu phases, which have a nearly identical composition of s-(-9)-100% and s-(-9)-60%.

Table S1. The ICP-OES measured value of loading amount of NiC_x on Ni/CF substrate, and its respective Ni and C loading amount for s-(-9)-100% (d-$NiC_{0.2}$NS/Ni/CF), s-(-10)-100%, s-(-8)-100%, s-(-9)-80%, and s-(-9)-60%. The molar ratio (Ni : C) and C content of NiC_x on Ni/CF substrate for s-(-9)-100%, s-(-10)-100%, s-(-8)-100%, s-(-9)-80%, and s-(-9)-60%.

Sample	m(NiC_x) (mg cm^{-2})	m(Ni) (mg cm^{-2})	m(C) (mg cm^{-2})	Molar ratio (Ni : C)	C content
s-(-9)-100%	2.74	2.63	0.11	1 : 0.20	16.7 at%
s-(-10)-100%	2.86	2.69	0.17	1 : 0.30	23.1 at%
s-(-8)-100%	2.83	2.75	0.08	1 : 0.14	12.3 at%
s-(-9)-80%	2.90	2.78	0.12	1 : 0.21	17.4 at%
s-(-9)-60%	2.84	2.77	0.11	1 : 0.19	16.0 at%

Table S2. Comparison of the electrocatalytic performance of d-$NiC_{0.2}$NS/Ni/CF versus bifunctional water splitting electrocatalysts reported recently.

Catalyst	Reaction	Electrolyte Solution	Current density (j)	Overpotential at the corres-ponding j	Stability test	Reference
NiC_x/CF	HER	1M KOH	10 mA/cm^2	121 mV	100 h	This work
	OER		10 mA/cm^2	228 mV	100 h	
Co-P/CF	HER	1M KOH	10 mA/cm^2	94 mV	24 h	*Angew. Chem. Int. Ed.* **2015**, *54*, 6251-6254
	OER		10 mA/cm^2	345 mV	24 h	
Ni_5P_4/NF	HER	1M KOH	10 mA/cm^2	150 mV	20 h	*Angew. Chem.*, 2015, 54, 12538-12542
	OER		10 mA/cm^2	290 mV	20 h	
Ni_3S_2/NF	HER	1M KOH	10 mA/cm^2	223 mV	200 h	*J. Am. Chem. Soc.* **2015**, 137, 14023−14026
	OER		10 mA/cm^2	260 mV	200 h	
NiSe/NF	HER	1M KOH	20 mA/cm^2	96 mV	12 h	*Angew. Chem. Int. Ed.* **2015**, *54*, 9351–9355
	OER		20 mA/cm^2	270 mV	12 h	
EG/$Co_{0.85}$Se /NiFe-LDH	HER	1M KOH	10 mA/cm^2	260 mV	10 h	*Energy Environ. Sci.* **2016**, 9, 478-483
	OER		150 mA/cm^2	270 mV	10 h	
ONPPGC /OCC	HER	1M KOH	10 mA/cm^2	446 mV	10 h	*Energy Environ. Sci.* **2016**, 9, 1210-1214
	OER		10 mA/cm^2	410 mV	10 h	
CoP/rGO	HER	1M KOH	10 mA/cm^2	150 mV	~22 h	Chem. Sci. **2016**, 7, 1690-1695
	OER		10 mA/cm^2	340 mV	~22 h	
Co_9S_8@MoS_2 /CNFs	HER	0.5M H_2SO_4	10 mA/cm^2	190 mV	~9 h	Adv. Mater. **2015**, 27, 4752-4759
	OER	1M KOH	10 mA/cm^2	430 mV	10 h	
Co-P/NC	HER	1M KOH	10 mA/cm^2	154 mV	24h	Chem. Mater., 2015, 27, 7636-7642
	OER	1M KOH	10 mA/cm^2	319 mV	24h	

Table S3. The geometric values of series resistance (R_s) and charge transfer resistance (R_{ct}).

Sample	R_s (Ω)	R_{ct} (Ω)
s-(-9)-100%	6.21	76.79
s-(-10)-100%	6.39	154.1
s-(-8)-100%	5.61	66.06
s-(-9)-60%	6.26	80.03

References

1 J. Xie, S. Li, X. Zhang, J. Zhang, R. Wang, H. Zhang, B. Pan and Y. Xie, *Chem. Sci.*, 2014, 5, 4615-4620.

2 L. Feng, G. Yu, Y. Wu, G. Li, H. Li, Y. Sun, T. Asefa, W. Chen and X. Zou, *J. Am. Chem. Soc.*, 2015, 137, 14023-14026.

3 Y. Zhou, R. Ma, P. Li, Y. Chen, Q. Liu, G. Cao and J. Wang, *J. Mater. Chem. A*, 2016, 4, 8204-8210.

4 M. Browne, S. Stafford, M. O'Brien, H. Nolan, N. Berner , G. Duesberg, P. Colavita and M. Lyons, *J. Mater. Chem. A*, 2016, 4, 11397-11407.

5 M. Gong, Y. Li, H. Wang, Y. Liang, J. Wu, J. Zhou, J. Wang, T. Regier, F. Wei and H. Dai, *J. Am. Chem. Soc.*, 2013, *135*, 8452–8455.

6 T. Ma, S. Dai, M. Jaroniec and S. Qiao, *Angew. Chem. Int. Ed.*, 2014, 53, 7281-7285.

7 F. Andrej, L. Jun, H. Lars, J. Ulf and M. Martin, J. Phys.: Condens. Matter, 2014, 26, 415501.

8 A. Mansour, Surf. Sci. Spectra, 1994, 3, 221-230.